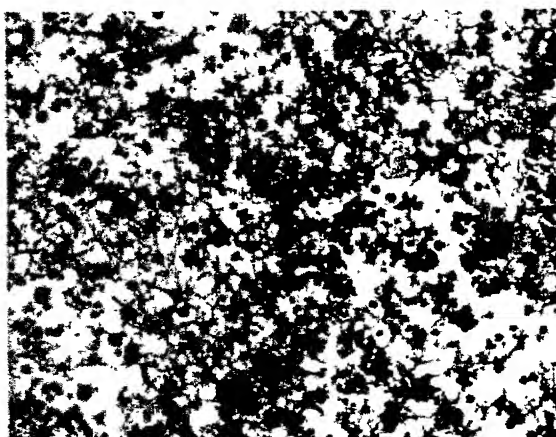


FIG. 1A



Top: No treatment

Bottom: Norepinephrine

FIG. 1B

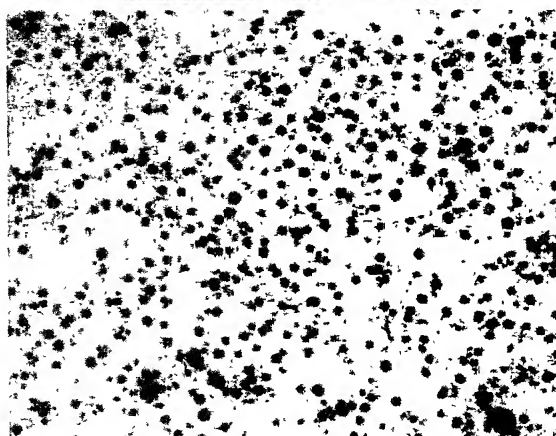
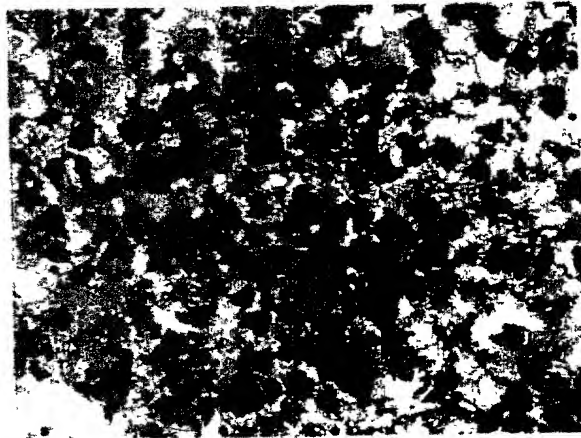
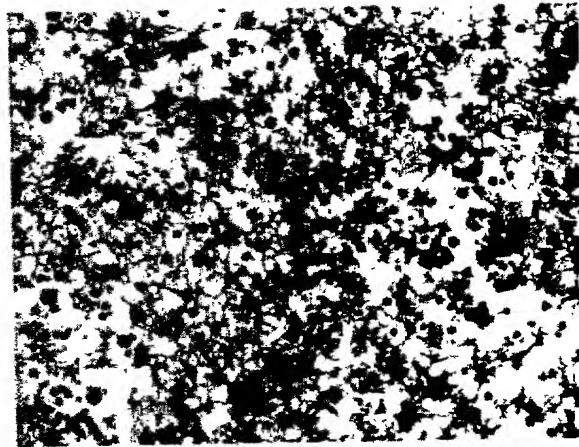


FIG. 2A

Top: No treatment

Bottom: Cholera toxin

FIG. 2B



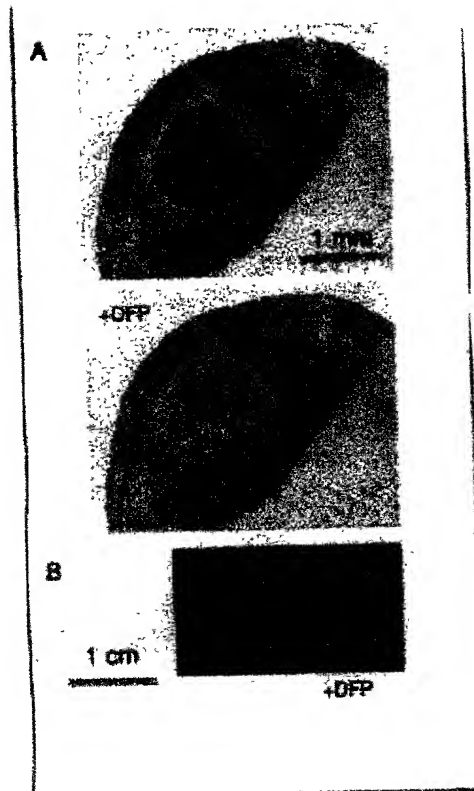


FIG. 3A

FIG. 3B

FIG. 3C

FIG. 4A

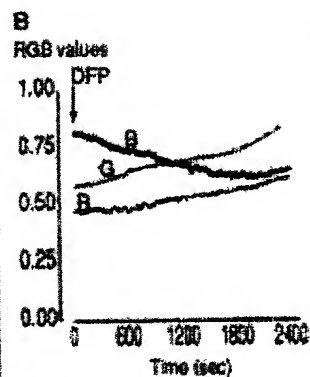
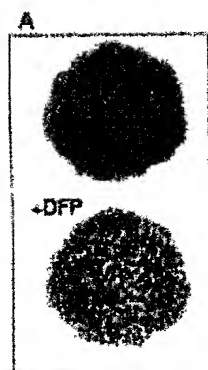


FIG. 4B

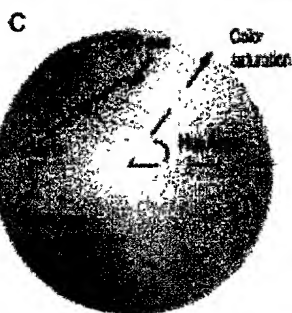


FIG. 4C

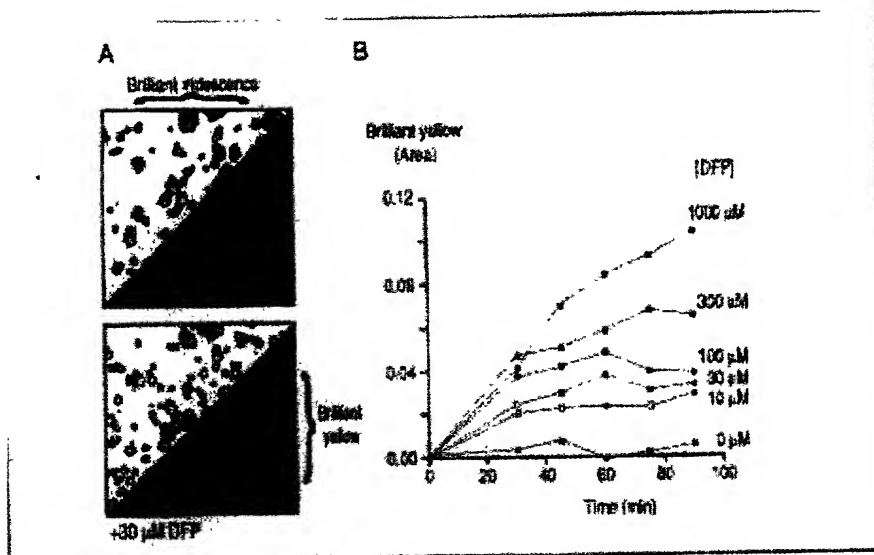
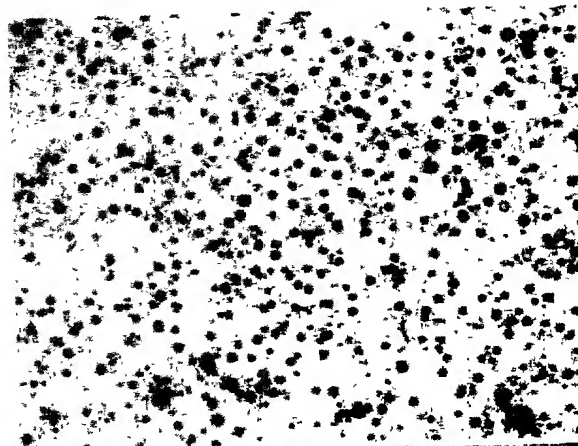


FIG. 5A

FIG. 5B

FIG. 6A



Top: No pre-incubation with cholera toxin, followed by norepinephrine

Middle: Pre-incubation with a threshold dose of cholera toxin, followed by norepinephrine

FIG. 6B

Bottom: Pre-incubation with a higher dose of cholera toxin, followed by norepinephrine.

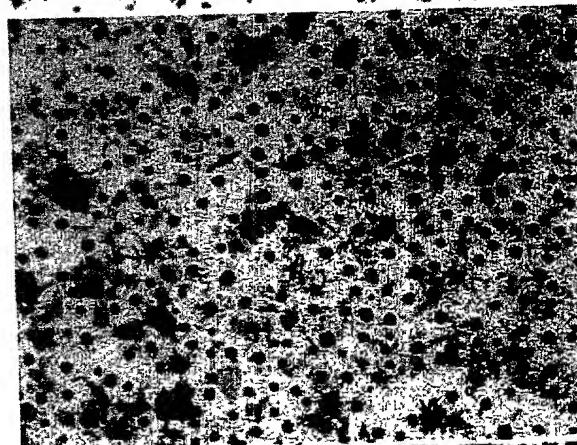
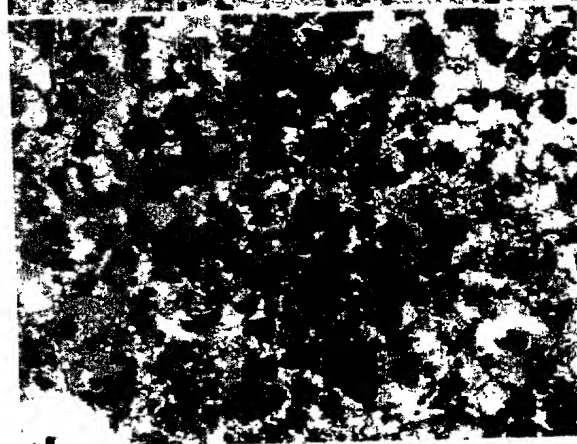


FIG. 6C

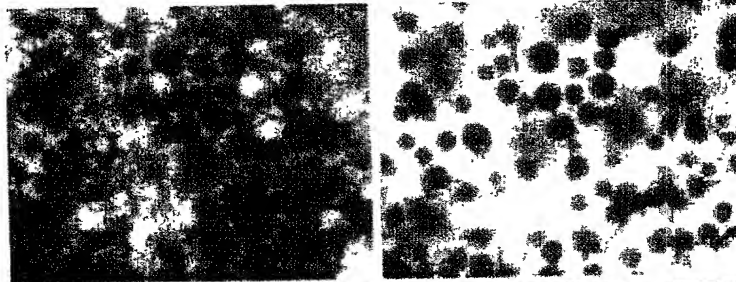


Before adding bacteria      After adding bacteria

FIG. 7A

FIG. 7B

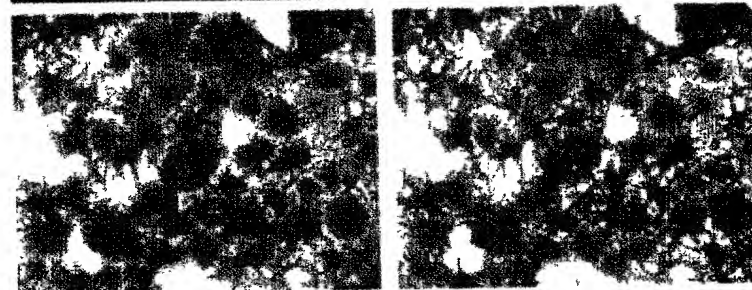
Strain 1



Strain 2

FIG. 8A

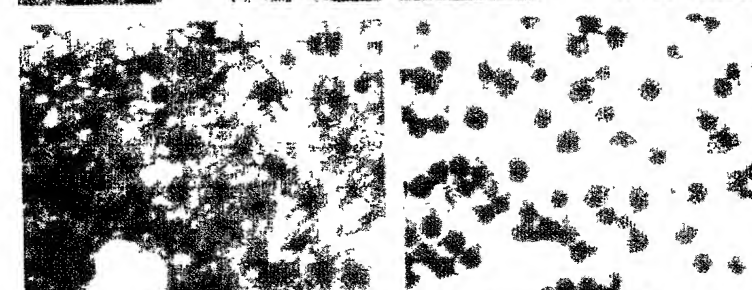
FIG. 8B



Strain 3

FIG. 9A

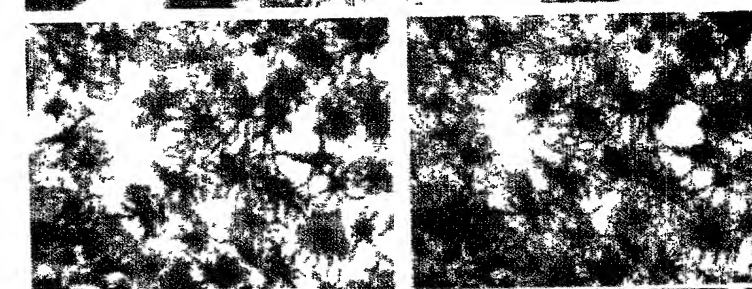
FIG. 9B



Strain 4

FIG. 10A

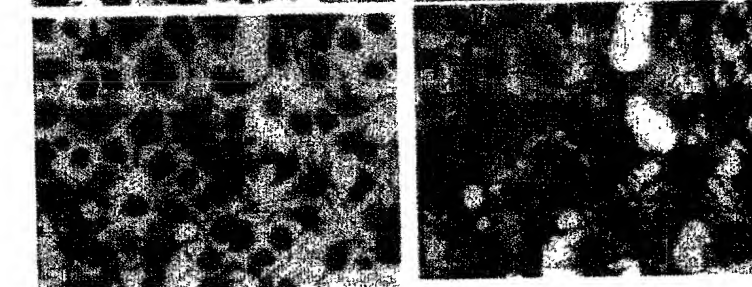
FIG. 10B



Strain 5

FIG. 11A

FIG. 11B



This is an example of a before (top)-and-after (bottom) shot of the effects of bacteria on cultured chromatophores.

FIG. 12A

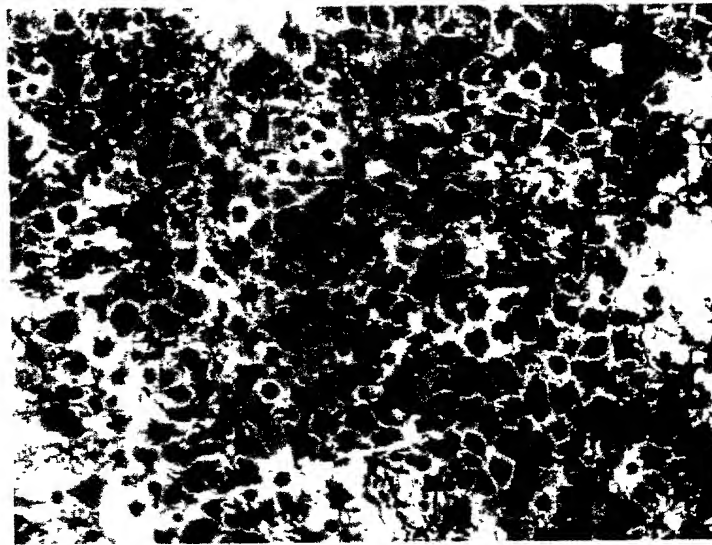
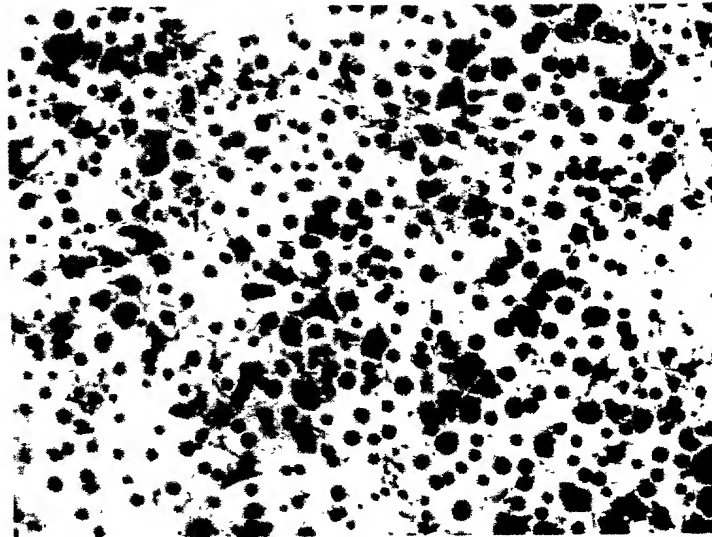


FIG. 12B























|         | Agent  | Chemical Type  | Effective dose | Direct Effects  | Challenge A (norepinephrine)   | Challenge B (forskolin)   |
|---------|--|--|----------------|---|--|---|
| Control | None   | -  | -              |  |  |  |
| I       | DFP<br>Mipafos<br>Paraoxon   | phosphorofluoridate<br>phosphorofluorodiamidate<br>phosphate   | ppm            |  |  |  |
| II      | FMSF<br>EPN  | sulfonylfluoride<br>phosphonothioate   | ppm            |  |  |  |
| III     | Mevinphos<br>Dichlorvos  | phosphate<br>phosphate   | ppt            |  |  |  |
| IV      | Trichlorfon  | phosphonate  | ppt            |  |  |  |
| V       | Chlorpyrifos<br>Fenitrothion<br>Merphos<br>Carbaryl<br>Methomyl<br>2,5 Hexanedione<br>Acrylamide | phosphorothioate<br>phosphorothioate<br>phosphotriethionate<br>carbamate<br>carbamate<br>diketone<br>amide | ND             |  |  |  |

FIG. 13

The appearance of chromatophore **sensor cells** varies according to their exposure to bioactive agents, as illustrated by these high-magnification examples.

FIG. 14A

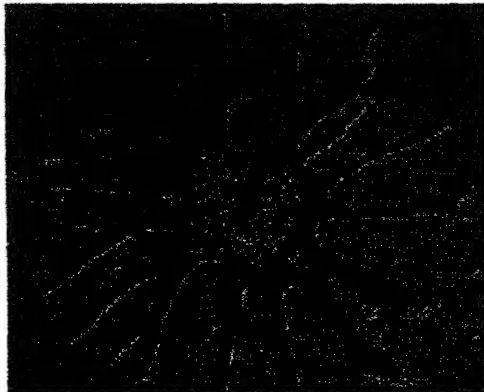


FIG. 14B

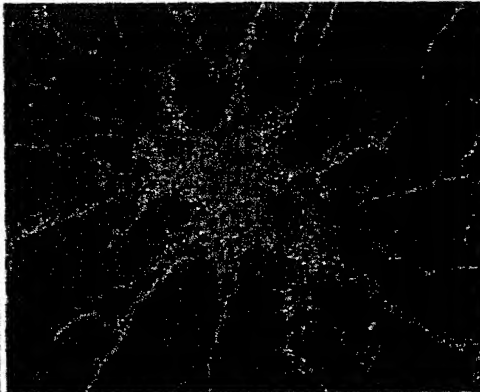


FIG. 14C

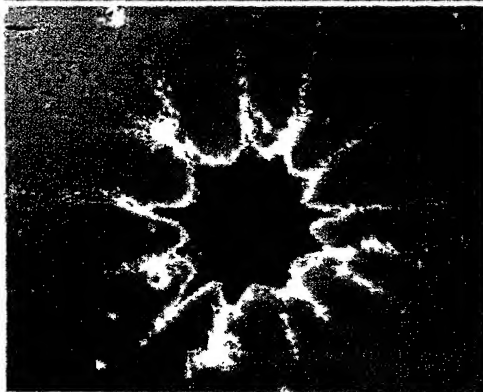


FIG. 14D

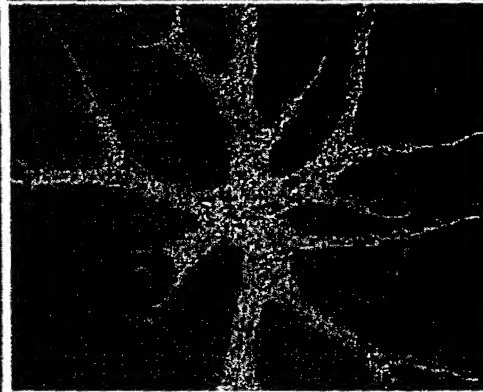


Figure 1. Species-comparison of chromatophore plating density and morphology. Top, *Betta splendens* chromatophores cultured on polystyrene. Bottom, *Hemichromis bimaculatus* chromatophores, cultured on polystyrene by identical methods. The same size bar applies to both images.

FIG. 15A

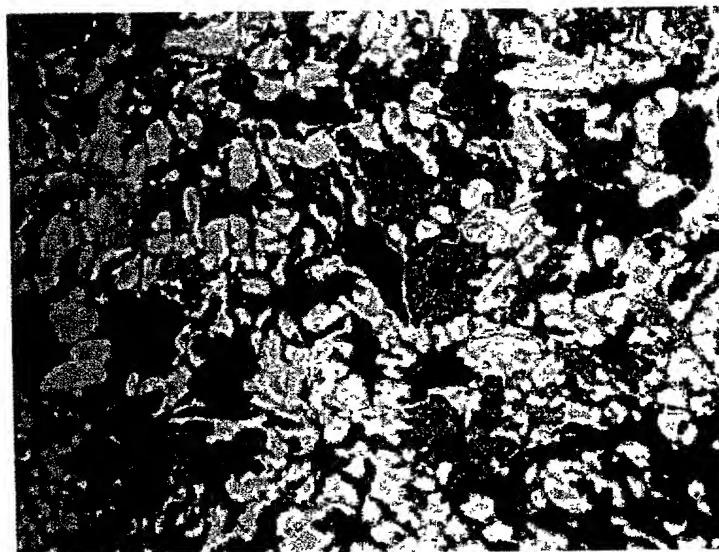
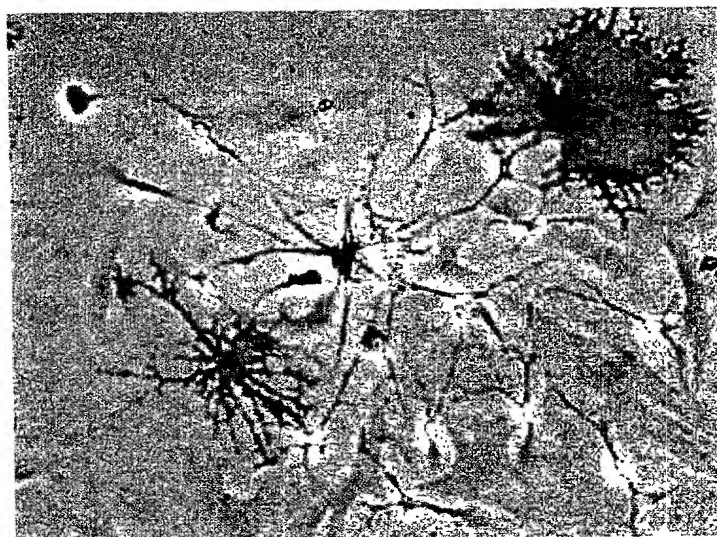


FIG. 15B



100 microns

Scales from three color variants of *Betta splendens*. These are basal colors, with no biologically active agent added.

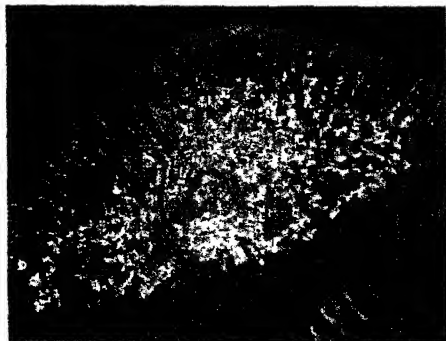


FIG. 16A



FIG. 16B



FIG. 16C

The cultured chromatophores from a Violet variant of *Betta splendens* were photographed with a dark-field background, a lighting technique which accentuates both the pigmented erythrophores and the blue-hued iridophores. This field of view shows the basal appearance of the cells, with no added biologically active agents.

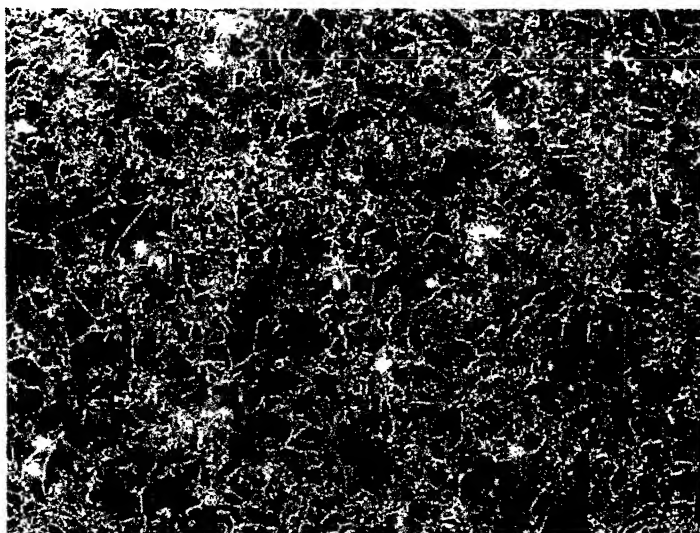


FIG. 17



## Hardware construction for the encapsulation of SOS sensor cells.

FIG. 18A



Extruder  
hardware  
(assembled)

FIG. 18B



FIG. 18C

Air-flow  
adjustment  
mechanism

Before

After 10nM  
Norepinephrine

FIG. 19A  
(+)  $\text{Ca}^{2+}$



FIG. 20A  
(-)  $\text{Ca}^{2+}$



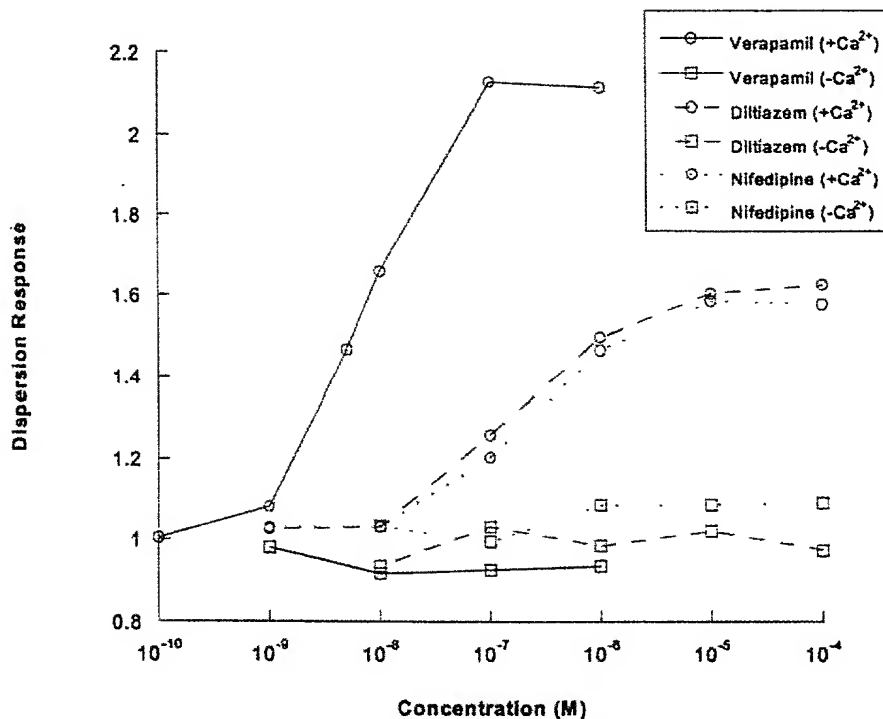
FIG. 19B



FIG. 20B



**Figure 1:** Demonstration of the dependence of  $\text{Ca}^{2+}$  on pigment aggregation in erythrocytes. (+)  $\text{Ca}^{2+}$  (first column): Performed in media containing 1.8 mM added  $\text{Ca}^{2+}$ . (-)  $\text{Ca}^{2+}$  (second column): Performed in media with no added  $\text{Ca}^{2+}$  plus 1mM EGTA. Before images were captured immediately prior to norepinephrine exposure and after images were captured 10 minutes after exposure.



**Figure 2:** Erythrocyte dose responses to L-type  $\text{Ca}^{2+}$  channel blockers verapamil, nifedipine, and diltiazem. Erythrocytes were treated at each data point with 1nM norepinephrine for at least 5 minutes prior to exposure of the channel blockers. The dispersion response was calculated as area occupied by the cells after chemical exposure for 10 minutes divided by the area occupied before exposure. (+)  $\text{Ca}^{2+}$  experiments were performed in PSS containing 1.8mM added  $\text{Ca}^{2+}$ . (-)  $\text{Ca}^{2+}$  experiments were performed in PSS with no added  $\text{Ca}^{2+}$  plus 1mM EGTA to demonstrate the requirement of extracellular  $\text{Ca}^{2+}$  for channel blockers to block inward movement of  $\text{Ca}^{2+}$  and thus cause direct dispersion of erythrocytes.

FIG. 21

FIG. 21

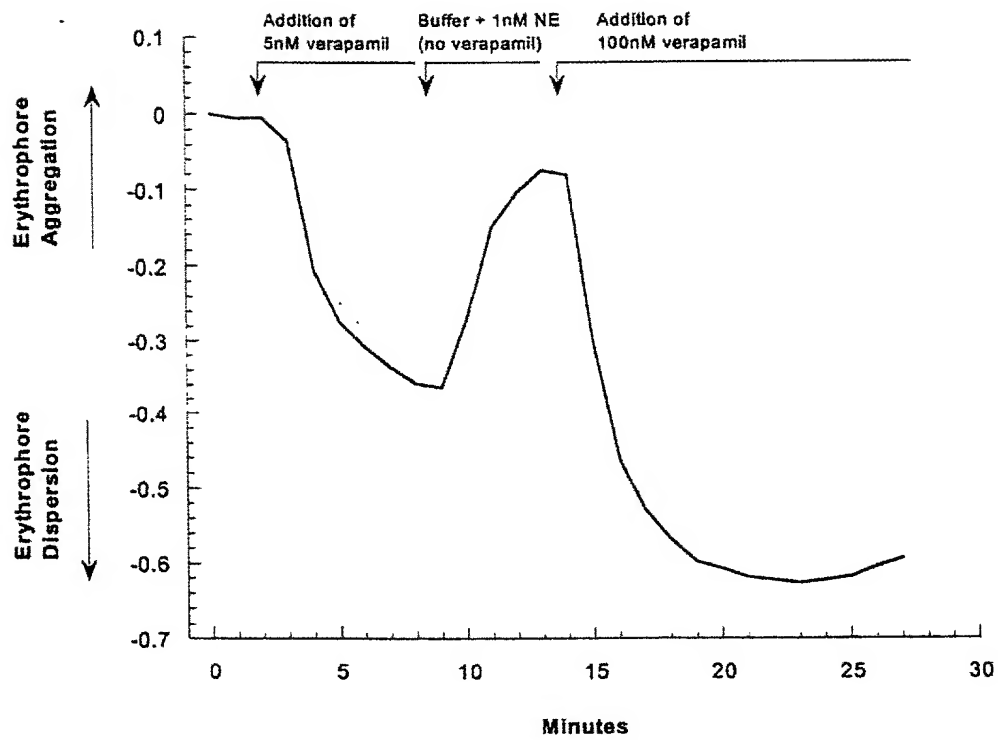


FIG. 22



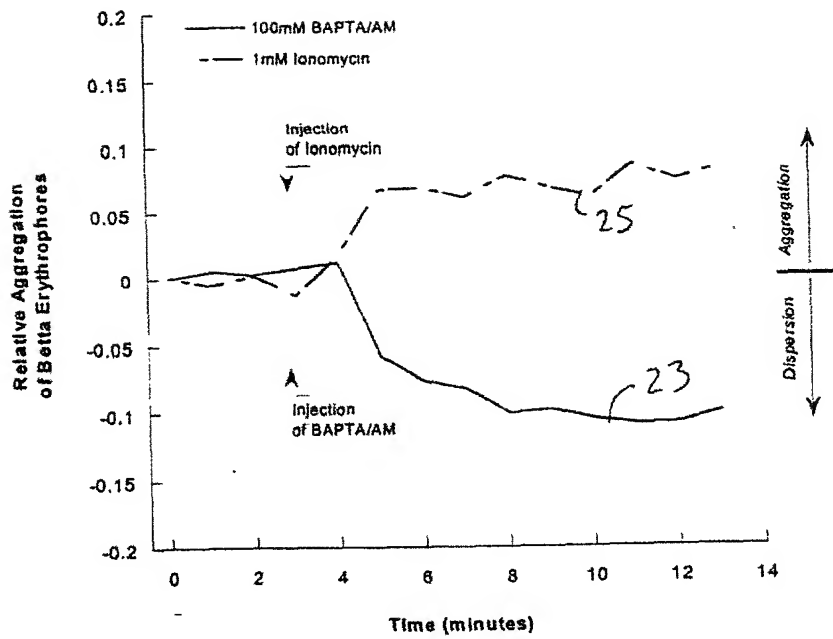
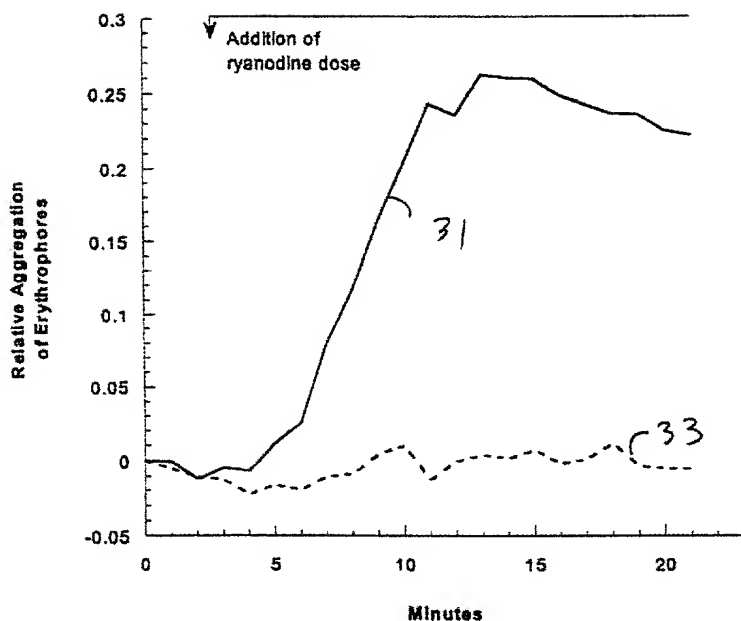


FIG. 23



**Aggregation response in Betta erythrocytes from ryanodine exposure at 10nM (solid line) and 10µM (dashed line) –** Ryanodine doses in PSS were added at the time point indicated and allowed to incubate with erythrocytes for the remainder of the experiment. Recent literature has indicated that ryanodine at doses  $<1\mu\text{M}$  are effective at stimulating  $\text{Ca}^{2+}$  release from the endoplasmic reticulum via ryanodine receptors; however, doses  $>1\mu\text{M}$  inhibit  $\text{Ca}^{2+}$  release through the same receptors. This data is consistent with these reports. The delay in initial erythrocyte response after dose addition may be the result of the time required for the molecule to pass through the plasma membrane and reach its intracellular target.

FIG. 24

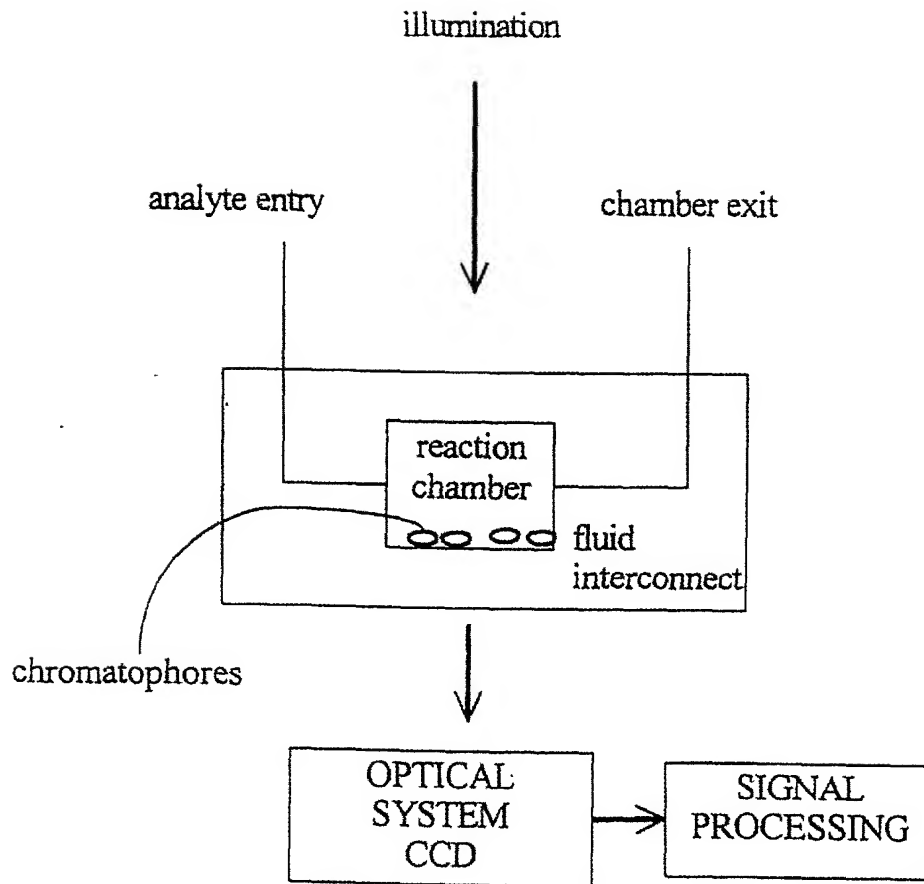


FIG. 25

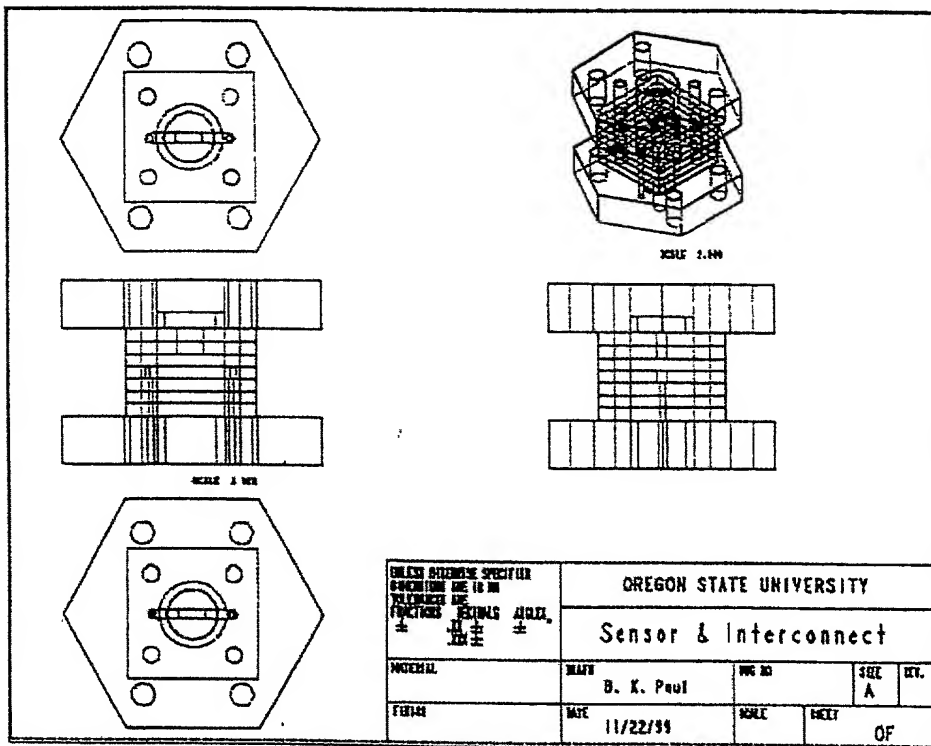
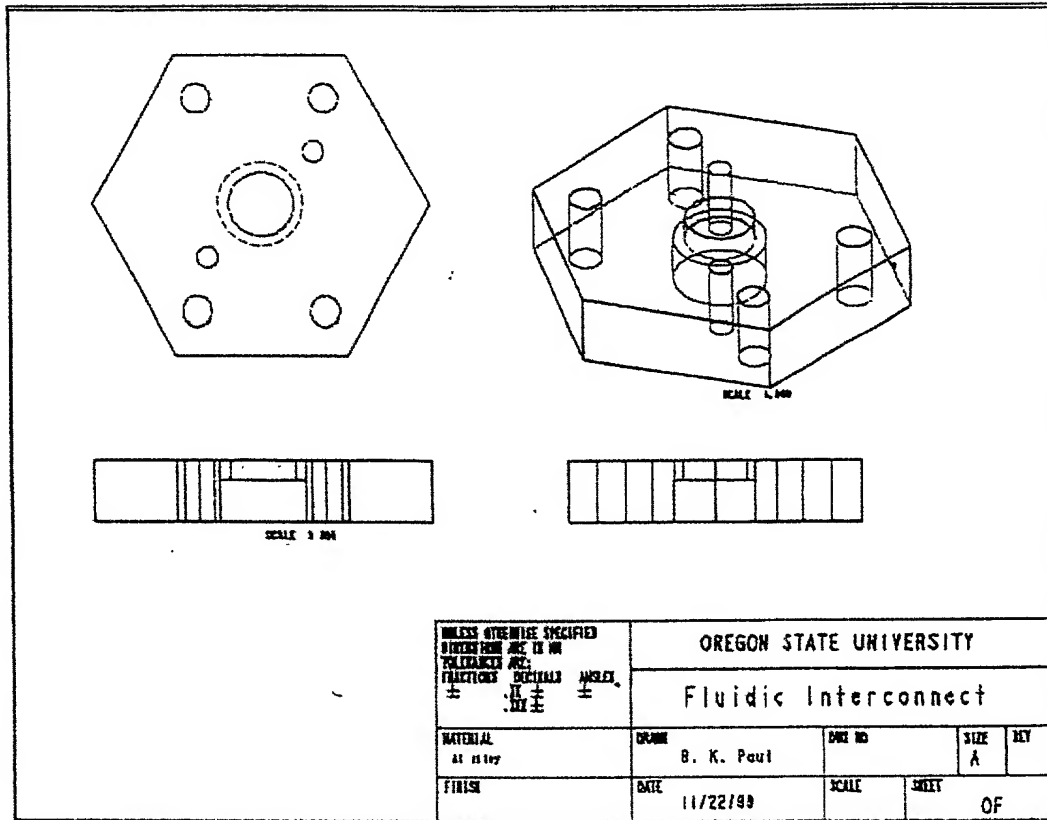


FIG. 26A



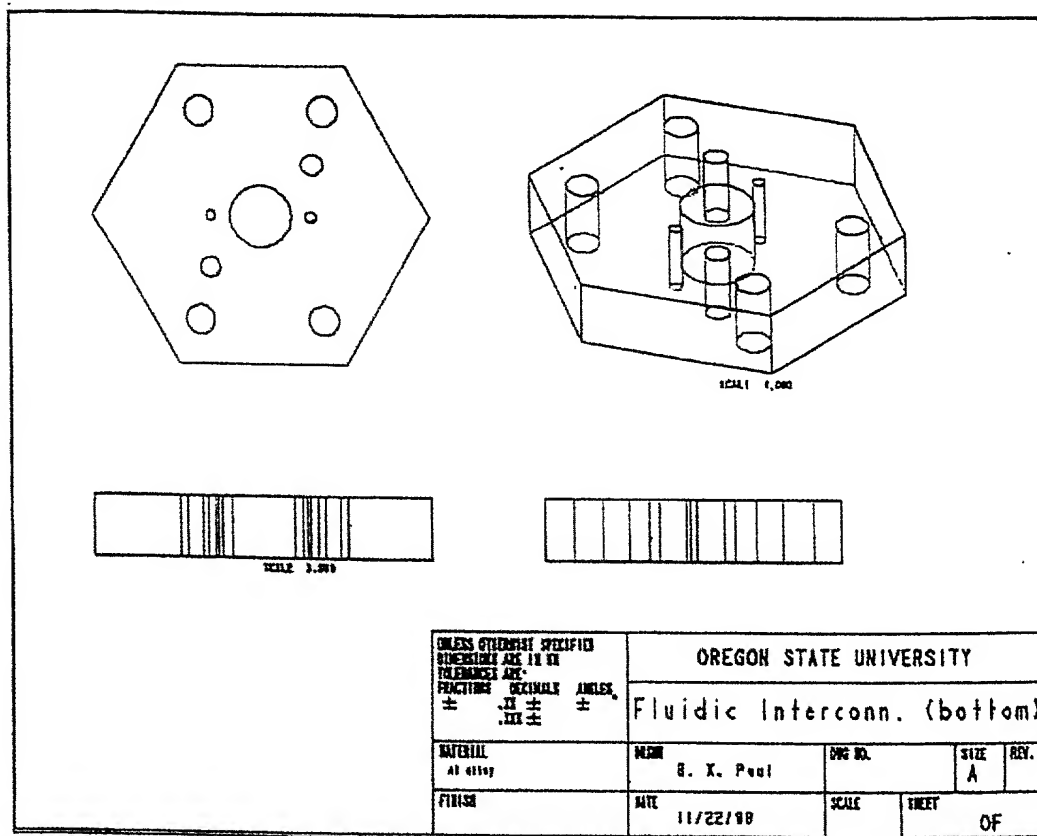
FIG. 26B

Engineering diagram and photograph of a cell chamber sandwiched within the fluidic interconnect. In the engineering diagram the thickness of the cell chamber has been exaggerated for clarity.

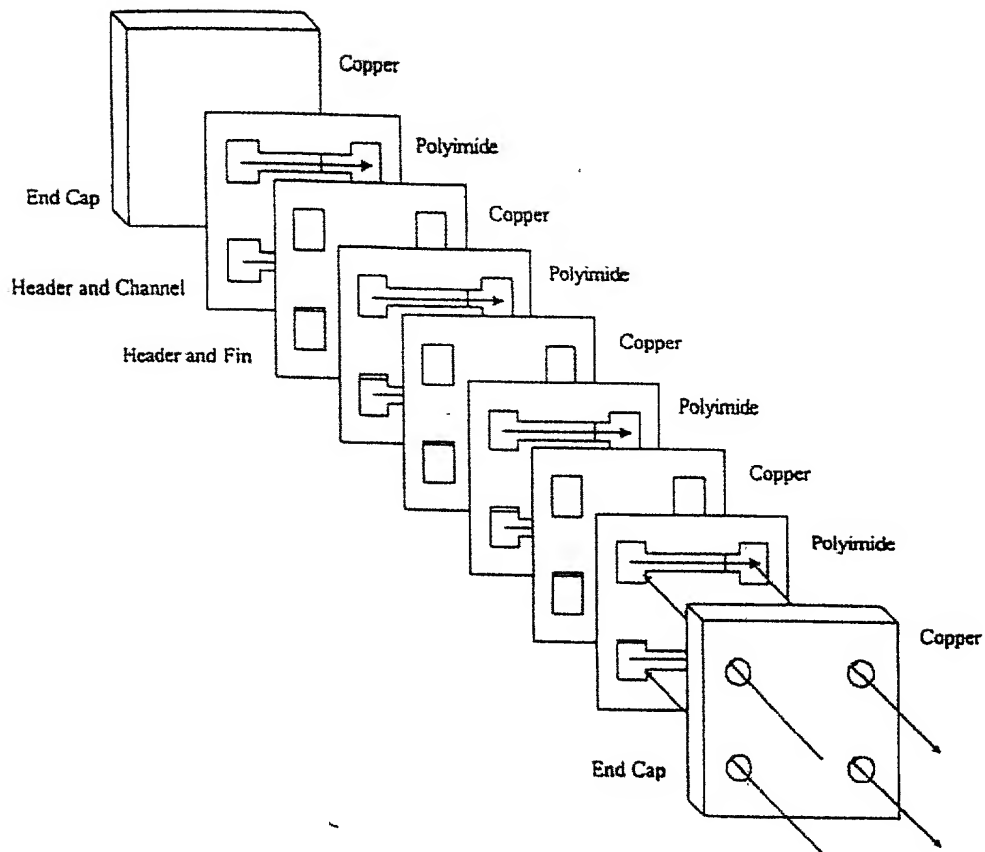


Engineering diagram showing one side of the fluidic interconnect.

FIG. 27



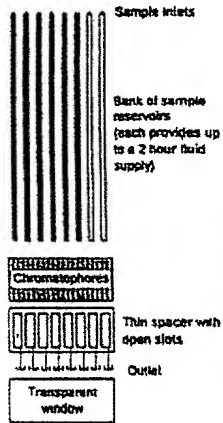
Engineering diagram showing the other side of the fluidic interconnect. The photograph shows both sides of the fluidic interconnect. Mounted on the left side of the interconnect is a transparent version of a cell chamber.



***Microlamination scheme used to fabricate a dual microchannel array. Arrows show direction of flow. In this case, laminae are bonded by use of the polyimide as a thermal adhesive.***

FIG. 29

Exploded view



Assembled view



Chamber detail

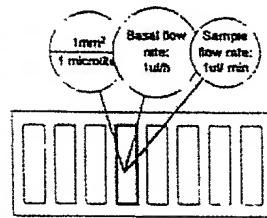


FIG. 30A

FIG. 30B

FIG. 30C



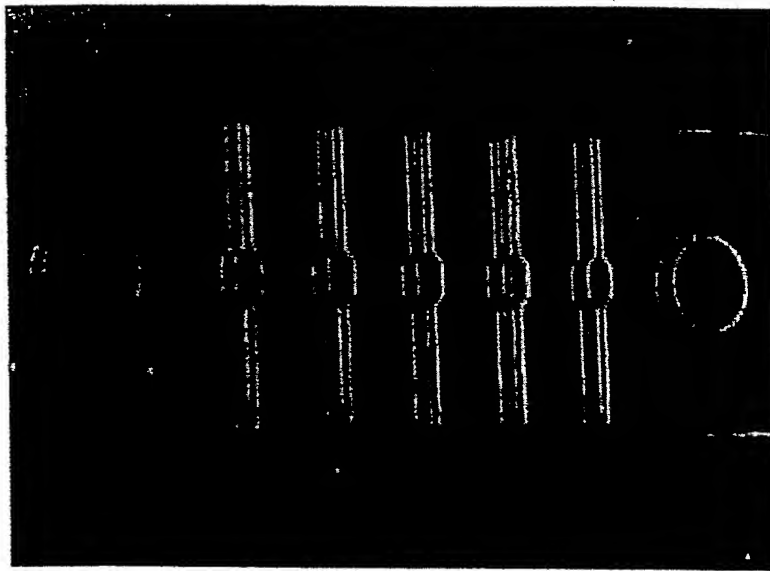


FIG. 31

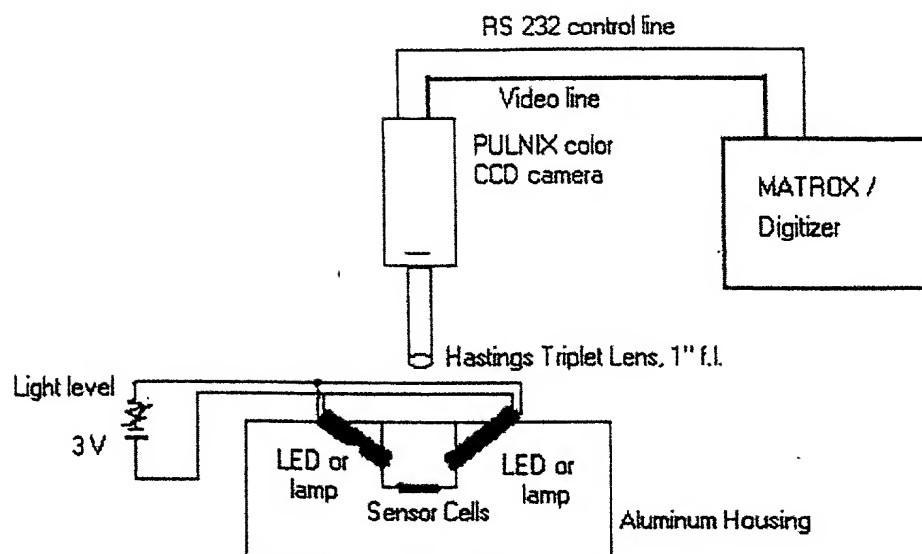


FIG. 32

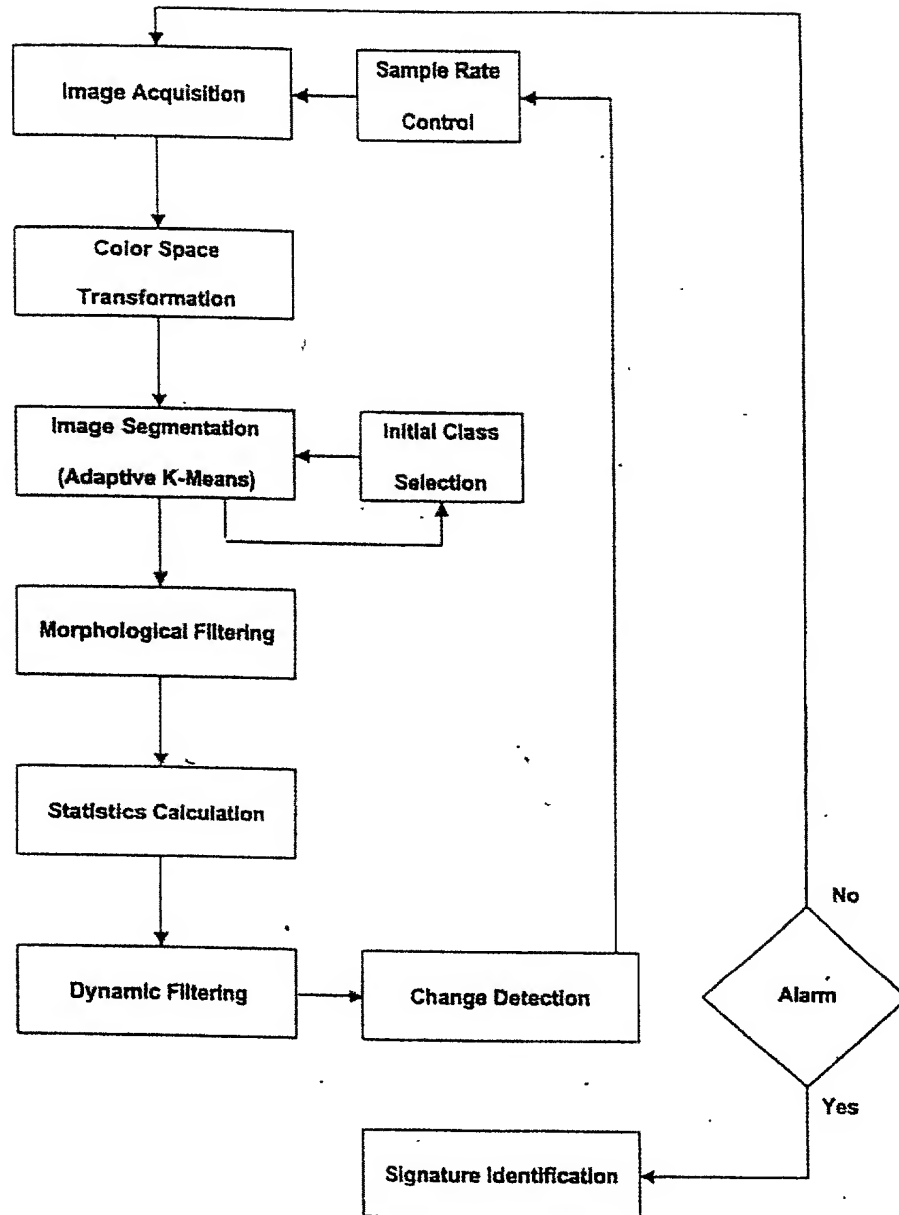


FIG. 33

A screen shot showing the output from the analyzer. The x-axis represents time (frame number). The y-axis represents an abstract count of cell color and morphology. The curve is essentially an indicator of the optical status of the sensor cells, and the dip in the plot occurring at frame 58 shows that the optical status changed. Indeed, norepinephrine had been injected into the cytosensor a few frames earlier. However, an x-y plot like this does not in itself provide a judgment call based on statistical probabilities. The algorithm therefore makes additional statistical calculations and reports those as the horizontal bar immediately above the x-y plot. That bar is colored green, except for a period of about 10 frames when it is colored red (from frame 58 to 68). The red color symbolizes the rejection of the null hypothesis, i.e. red means there was a greater than 99% probability that the sensor cells had changed their optical appearance. Thus, a judgment call has been made by the algorithm, and the red portion of the bar can be viewed as a positive alarm signal.

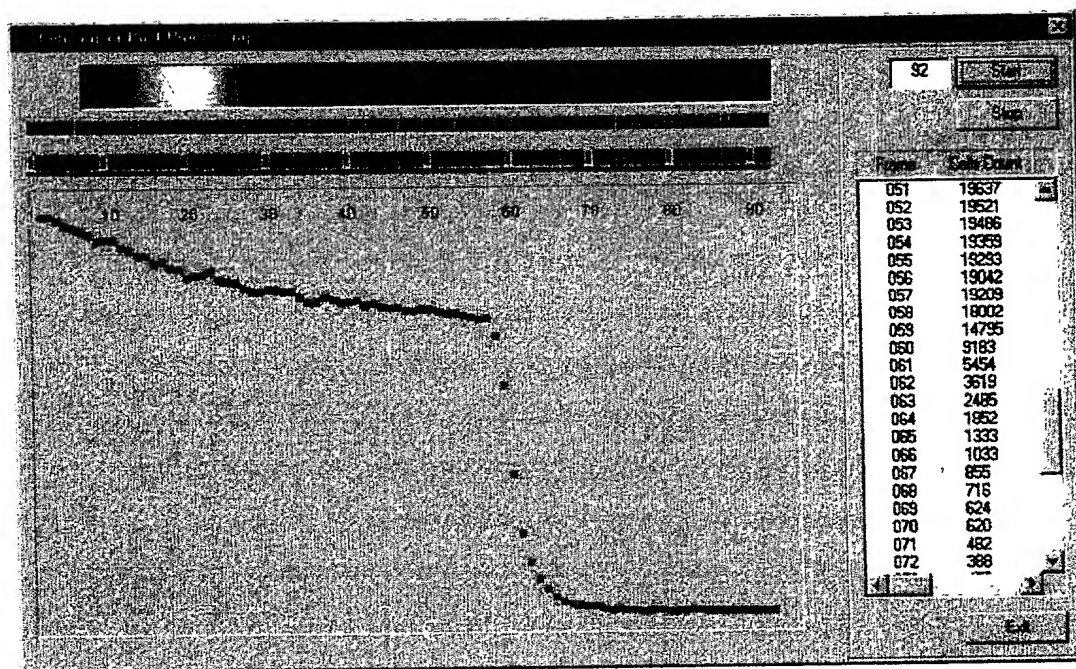


FIG. 34

## PARTICLE PRODUCTION

### Pressurized Vessel

1.5% sodium alginate and 95% water are mixed with ferromagnetic material and an active substance.

### Air Flow

Air flows down to tip of needle thereby shearing off a bead of desired size.

### CaCl<sub>2</sub> Bath

Bivalent Ca<sup>2+</sup> exchanges in for 2 Na<sup>+</sup> ions thus polymerizing the alginate material.

Length of time left in CaCl<sub>2</sub> bath determines extent of polymerization.

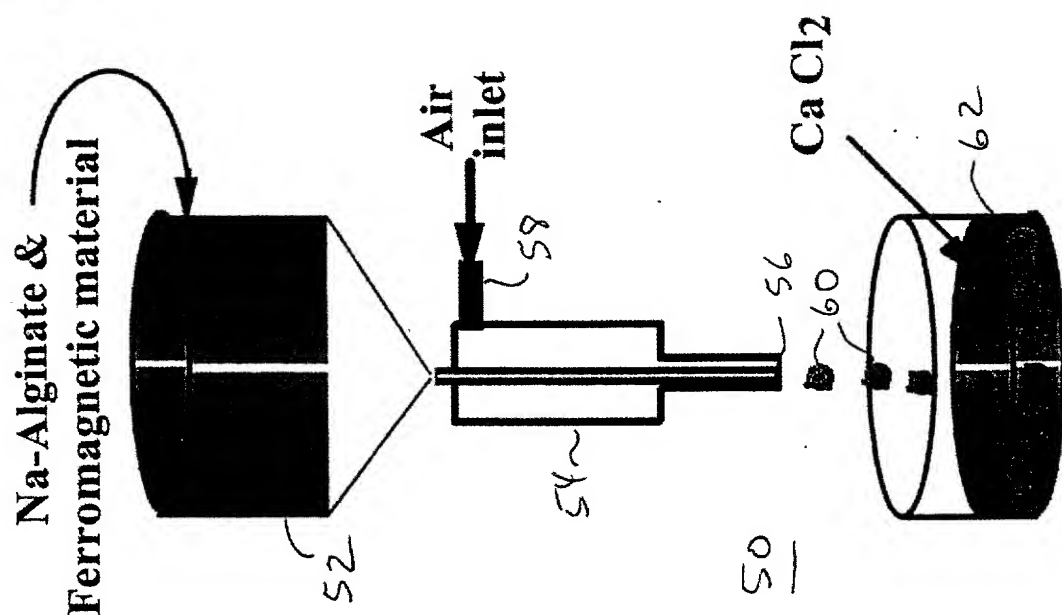


FIG. 35

Figure 1. Schematic representation of the apparatus for the extrusion of ferromagnetic particles.

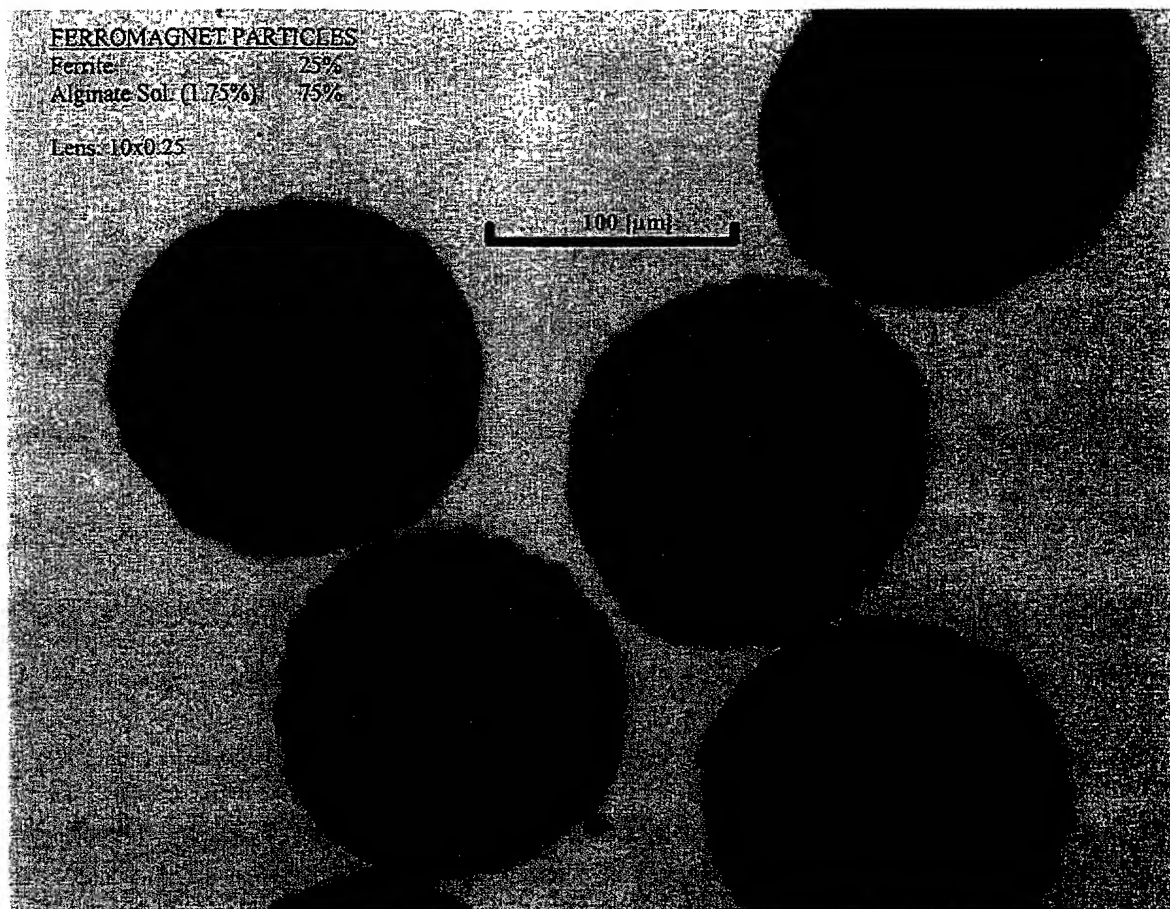


FIG. 36

Ferromagnetic micro-ball particles ( $d_p \approx 150 \mu\text{m}$ ) produced in apparatus shown in Figure 35 (ferrite content 25%, alginate solution 75%).

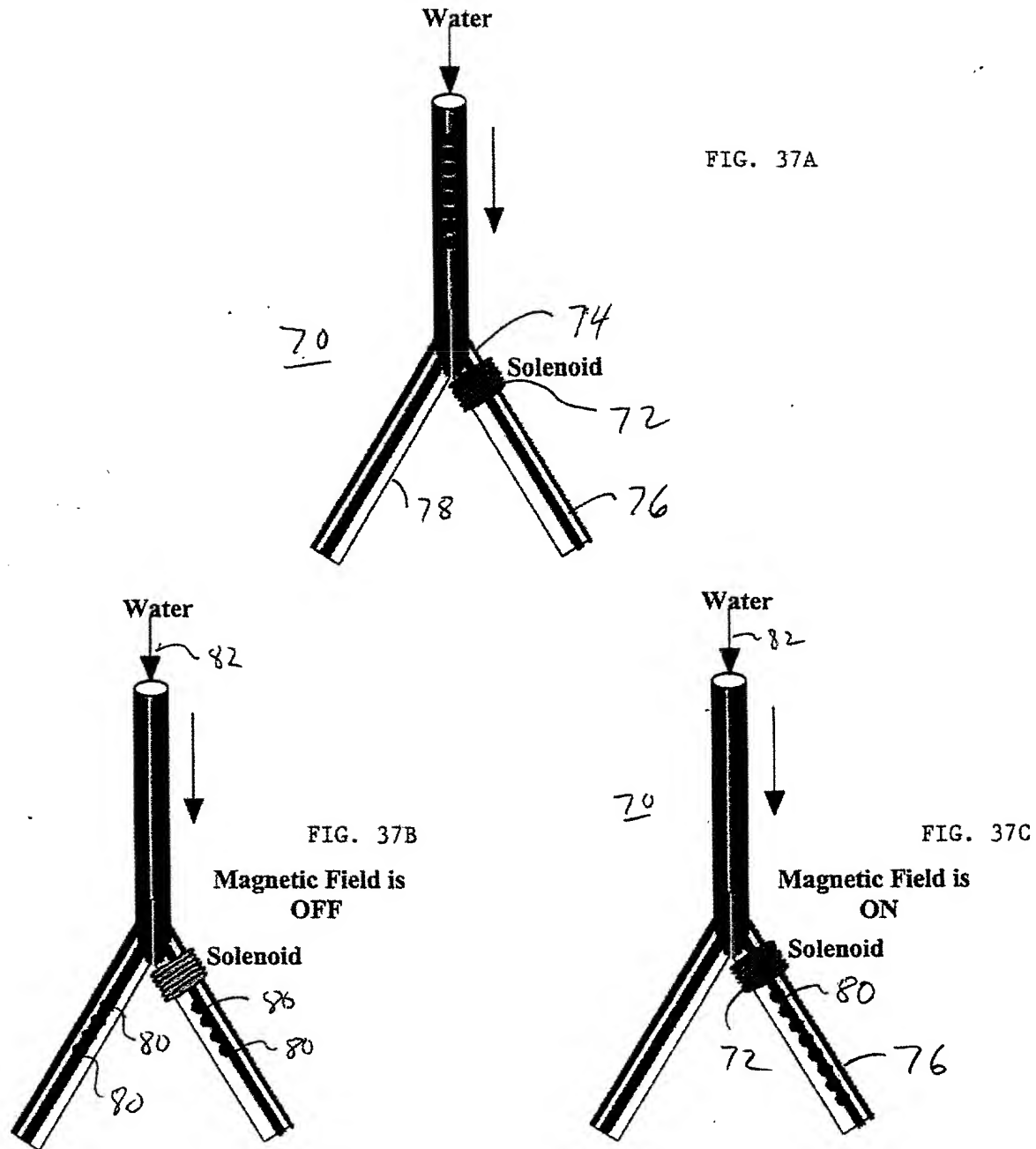


Figure 3. Schematic representation of the construction and operation of the magnetic gate.

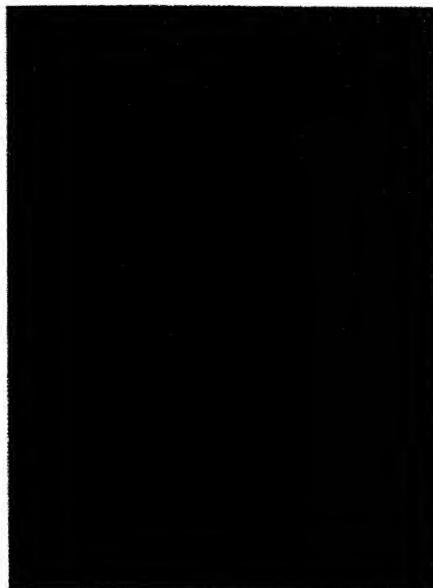


FIG. 38A

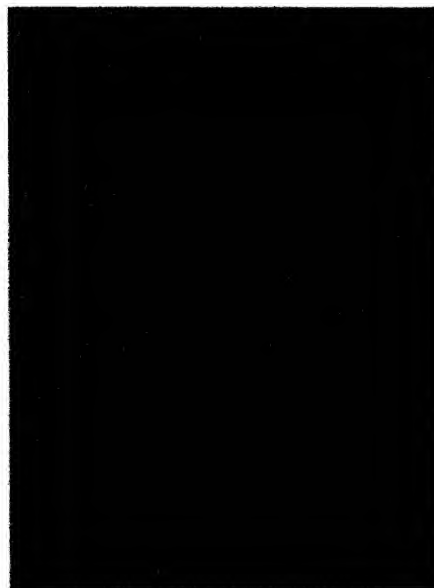


FIG. 38B

a) b)  
Micrograph of the mask: a) round coil; and b) square coil.

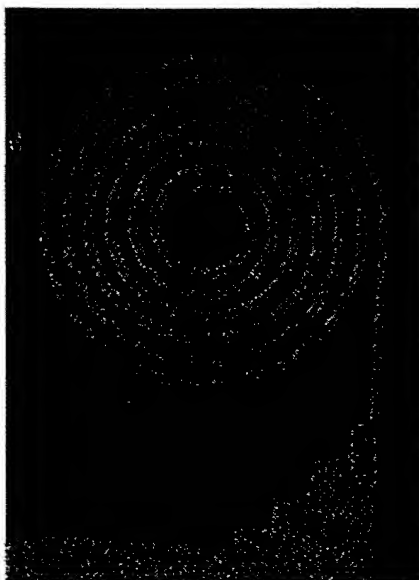


FIG. 39

Micrograph of a 5 micron high coil made by electroforming into a lithographic mold.



FIG. 40A

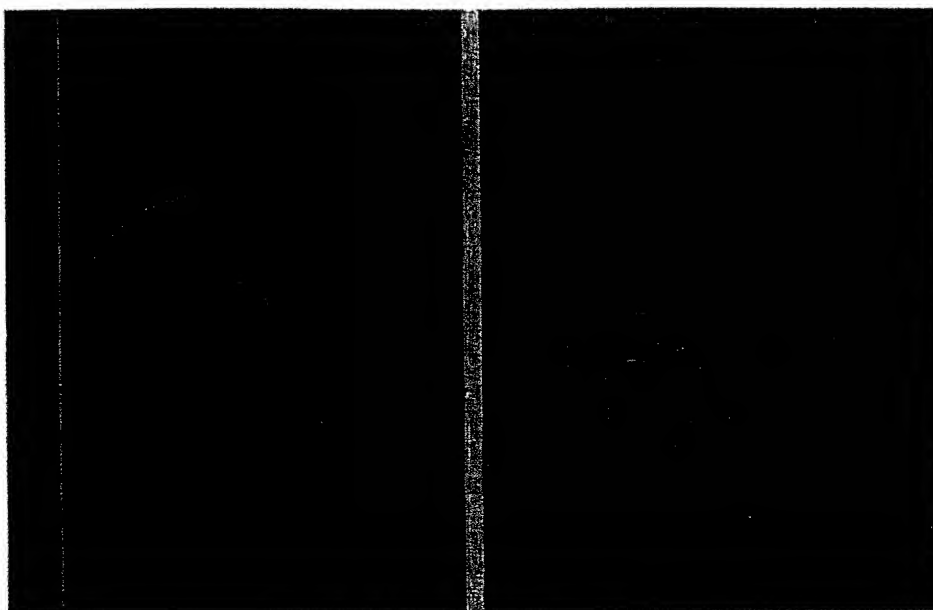


FIG. 40B

a)

b)

Micrograph of the one-way micro-ball-valve: a) orifice; and b) catch plate.

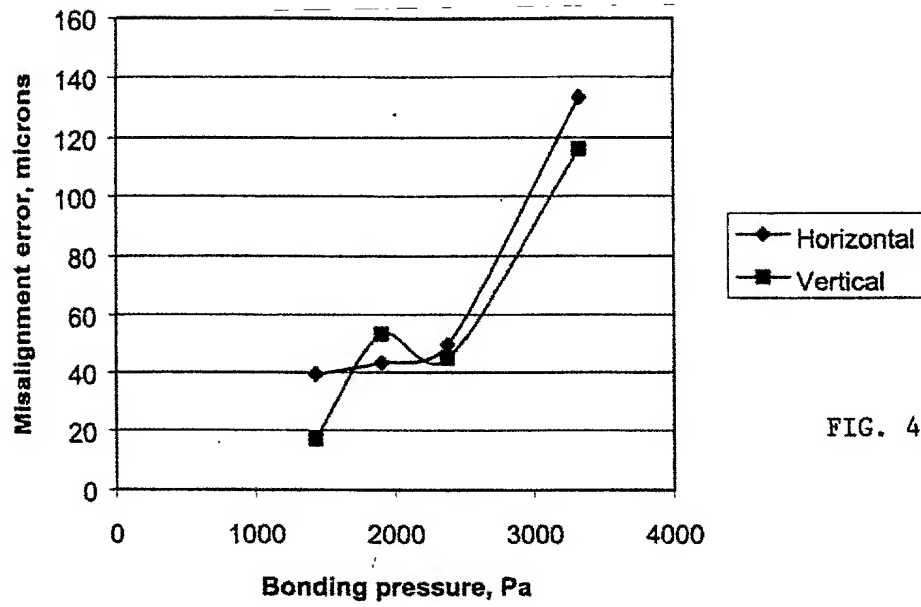


FIG. 41

Results showing effect of bonding pressure on misalignment error.

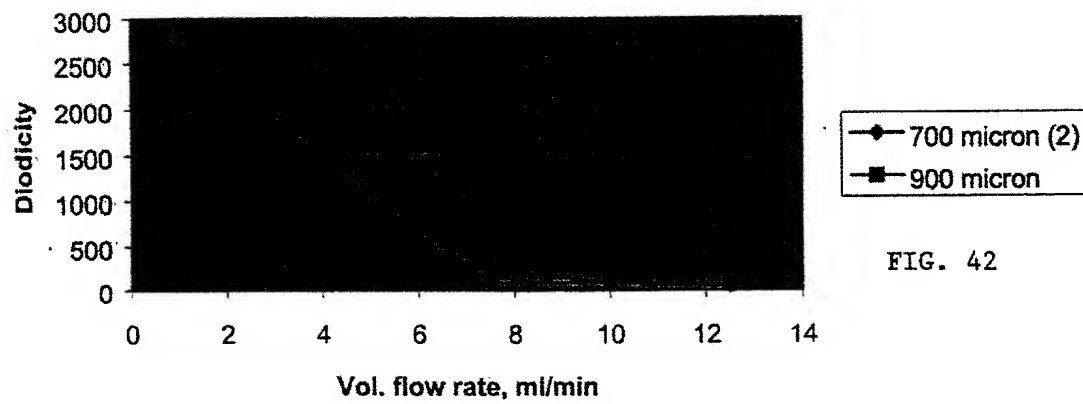


FIG. 42

Diodicity results for the last three micro-ball-valves.

Sandwich TOP VIEW  
 with  $\frac{1}{16}$  PORTS 180

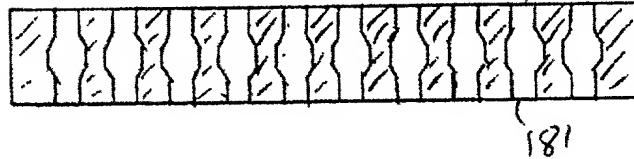


FIG. 43A

Layers TOP VIEW

$\frac{1}{8} \times \frac{1}{4} \times 3.3$



FIG. 43B

Top

$0.0X \times \frac{1}{4} \times 3.3$

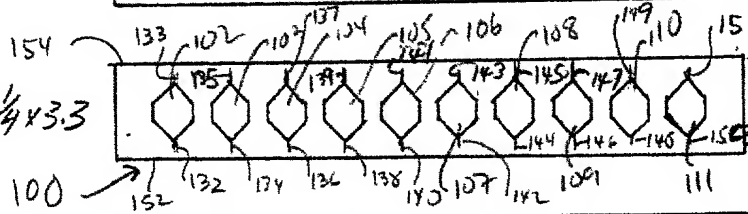


FIG. 43C  
 Chambers

$\frac{1}{8} \times \frac{1}{4} \times 3.3$

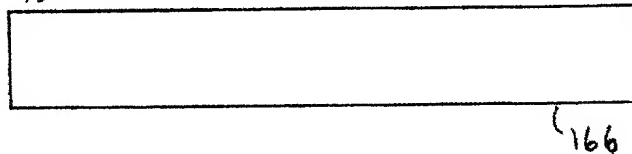


FIG. 43D  
 BOTTOM

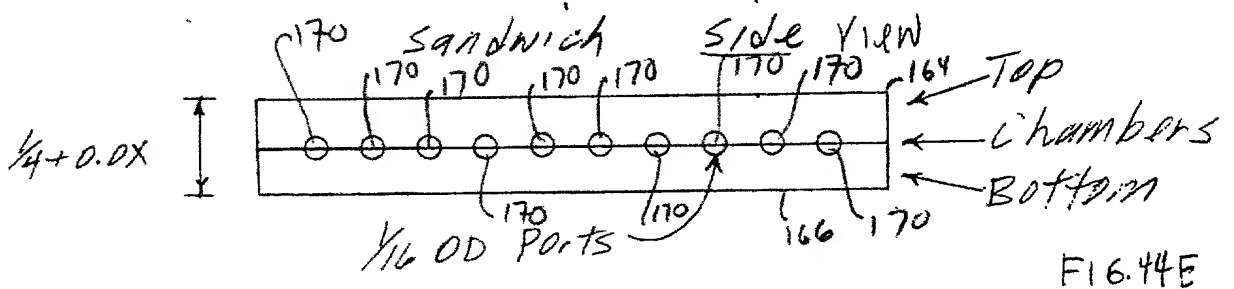


FIG. 44E